Proceedings World Geothermal Congress 2023
Beijing, China, April 17 – 21, 2023

Performance analysis of multi-source district heating system integrated with geothermal sources and energy storage

Jun Gao[1], Yuan Zhao[1], Shiji Yin[1], Dabiao Wang[2], Ruirui Zhao[3], Chen Liu[3], Zhiwei Yue[1], and Baomin Dai[3,*]

1. Powerchina HuaDong Engineering Corporation Limited, Hangzhou, 311122, China

2. National Engineering Research Center of Chemical Fertilizer Catalyst (NERC-CFC), School of Chemical Engineering, Fuzhou University, Fujian, 350108, China

3. Tianjin Key Laboratory of Refrigeration Technology, Tianjin University of Commerce, Tianjin, 300134, China

dbm@tjcu.edu.cn

Keywords: Geothermal sources, Air source heat pump, Energy storage, Integrated energy system, District heating.

ABSTRACT

District integrated heating technology combined with renewable energy is an effective way to achieve the goal of peak carbon emissions and carbon neutrality. Based on geothermal sources, air source heat pumps, and inter-seasonal energy storage technology, a multi-source integrated district heating system is proposed, which can meet the requirement of space heating in buildings. Taking a residential community with an area of 35700 m^2 as the application scenario, the thermal resistance- thermal capacity node network model (TRCM) of the borehole field and the thermodynamic model of the heat pump are developed. Then, the energy consumption and carbon emission performance of the heating system are achieved. The results indicate that the primary energy consumption of the multi-source district heating system is 45.73% less than the coal-fired boiler and the carbon emission reduces 787.83 t_{CO2}. The multi-source heat pump system can achieve social benefit, with the help of reasonable dispatching between the source and load side, and the contribution of renewable energy. The long-term stable operation of the energy system can be achieved. This study can provide a theoretical reference for the development of integrated energy systems combined with geothermal energy.

1. INTRODUCTION

From the perspective of global energy consumption, building energy consumption accounts for up to 36% of the overall social energy demand, and building carbon emissions account for up to 39% throughout the whole society[1]. Reducing energy consumption for space heating is one of the key solutions to effectively reduce carbon emissions. To reduce carbon emissions, the Paris Agreement calls for the global average temperature rise to be controlled within 2°C[2]. China has also responded to the international agreement to set the goal of "carbon peaking" and "carbon neutrality"[3]. The Clean Heating Plan for Winter in Northern China (2017-2021) requires that geothermal sources and other renewable energy should be selected due to the practical local conditions[4]. The 14th Five-Year Plan for Modern Energy System requires that the development of geothermal sources for heating and refrigeration should be actively promoted[5]. The idea of "geothermal source +" has been widely recognized.

Although there has been an extensive study of ground source heat pumps in building energy savings, there is a problem of soil heat imbalance. As for the air source, the building heating demand cannot be met when the ambient temperature is low in winter. The proper configuration of ground source heat pumps and air source heat pumps can be used for space heating (SH), domestic hot water (DHW), geothermal thermal release, and energy storage to meet various demands. Due to the advantages of multi-source complementarity, there are more and more researches on system optimization and design to meet the requirement of building space heating and domestic hot water. Emmi et al.[6] study the coupling system of air source, solar energy, and ground source heat pump. The study indicated that the energy efficiency of the multi-source system increased by 16-25% compared with the ordinary air-water heat pump system. Grossi et al.[7] constructed a multi-source system coupled with a geothermal source and air source, and analyzed the seasonal and annual performance factor of the dual-source heat pump (DSHP). It was found that the borehole heat exchanger length coupled to the heat pump was reduced by 30-50% compared to the geothermal source only. Jia et al.[8] proposed a hybrid ground-coupled heat exchanger (HGCHE) system that combined with radiative sky cooling radiators (RSCR). The study showed that the thermal efficiency of RSCR assisted GCHE systems was 6.6% higher than GCHE systems. Nordgard-hansen et al.[9] proposed a mixed integer linear programming model to optimize the scale and operation of the system. The results show that the ground source heat pump system was beneficial to improve the sustainability of the energy system and its operation mode was related to the current feed-in price. Zheng et al.[10] proposed a photovoltaic (PV) auxiliary ground source heat pump and air source heat pump system (PVGSHP-ASHP) and evaluated its performance. The results showed that the optimized PVGSHP-ASHP consumed only 71,700 kWh of electricity per year.

Although the design of multi-source heat pump system is relatively mature, there are few studies on system performance and optimization. As a result, a multi-source district heating system is established. Meanwhile, the performance and operating modes of this system are investigated. Afterward, the primary energy consumption and carbon emissions of the studied system are compared with a conventional coal-fired boiler. A practical solution for the applications of residential space heating is provided by introducing the combination of multi-source complementary and energy storage technology.

2. MODLE DEVELOPMENT

2.1 System introduction

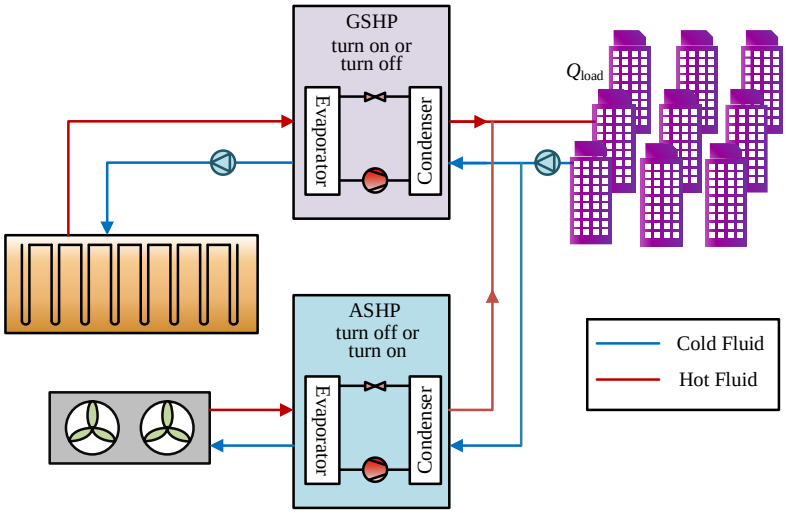

Figure 1: A multi-source heating system for building heating and domestic hot water.

Figure 1 depicts a schematic of a multi-source district heating system that integrates geothermal sources (GSHP), air source heat pumps (ASHP), and energy storage. The heat source of this system is mainly provided by the heat thermal stored in the soil and the thermal energy of the air. For this integrated system, when the energy efficiency of the ground source heat pump is lower than that of the air source heat pump system, the latter system will be on and the former will be off. Meanwhile, the technology of inter-seasonal energy storage is introduced due to the soil energy storage, indicating the thermal energy of the room in the summer can be stored in the soil, which can be extracted for space heating (SH) or domestic hot water (DHW) during the winter days. The operation mode of the district heating system is shown in Figure 2.

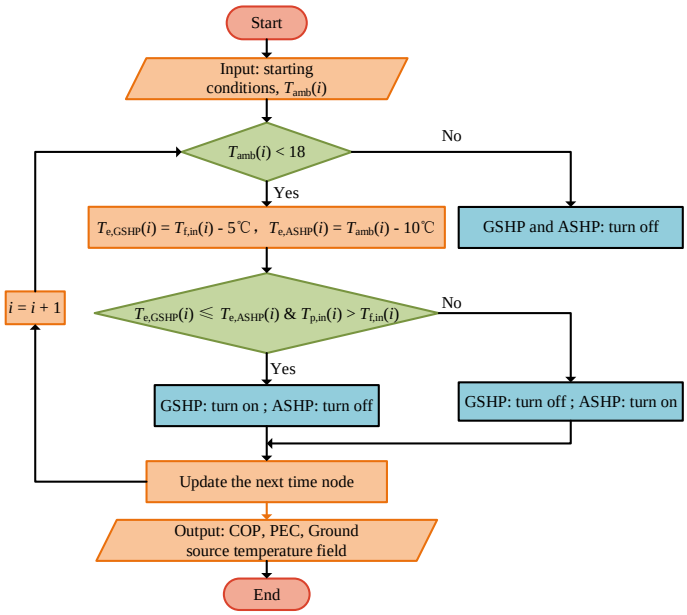

Figure 2: Flow chart of start-stop state of ground source heat pump and air source heat pump.

2.2 Mathematical modeling

2.2.1 Energy analysis model

The study scenario is based on an ordinary residence community with an area of 35700 m^2 in Beijing. The energy analysis model of the integrated energy system and the thermodynamic performance of the system are established in the following ways.

Hourly heat load at ambient temperature t_i is calculated as follows[11]:

$$L_H(t_i) = q_{H,Desi} \times \frac{t_{H,in} - t_i}{t_{H,in} - t_{H,Desi}} \quad (1)$$

where $q_{H,Desi}$, $t_{H,in}$, and $t_{H,Desi}$ is heating design heat load, indoor design temperature, and outdoor design temperature, respectively.

The heating seasonal total heat load (HSTL) and heating seasonal total energy consumption (HSTE) are calculated by the temperature bin-method:

$$\mathrm{HSTL} = \sum_{i=1}^{m} (L_{\mathrm{H}}(t_i) \times A_{\mathrm{H,Desi}} \times n_i) \tag{2}$$

$$\mathrm{HSTE} = \sum_{i=1}^{m} (W_{\mathrm{H}}(t_i) \times A_{\mathrm{H,Desi}} \times n_i) / f_{lost} \tag{3}$$

$$W_{\mathrm{H}}(t_i) = L_{\mathrm{H}}(t_i) / COP_{\mathrm{H}}(t_i) \tag{4}$$

where $A_{\mathrm{H,Desi}}$ is the total heating area, n_i, $W_{\mathrm{H}}(t_i)$, and $\mathrm{COP}(t_i)$ is the number of hours, power consumption, and COP at ambient temperature t_i, respectively.

2.2.2 Node network model

In this study, temperature nodes are successively established based on the control equation of mass and energy. The thermal resistance-heat capacity node network model (TRCM) borehole field is established as follows.

The general of each temperature node in the thermal resistance-thermal capacity network model is:

$$C_{\mathrm{j}} \frac{\mathrm{d}T_{\mathrm{j}}}{\mathrm{d}\tau} = \sum_{k=1}^{n} \frac{T_{\mathrm{k}} - T_{\mathrm{j}}}{R_{\mathrm{k}}} \tag{5}$$

where C is the heat capacity, ΔT and R is the temperature difference and the thermal resistance between two temperature nodes, respectively.

The axial geometric model is discretized by logarithmic series to improve numerical stability[12]:

$$z_{(j+1)} = z_{(j)} \cdot 10^{\left(\frac{\log_{10}(L/c_0)}{n_z}\right)} \tag{6}$$

where n_z is the number of discrete layers in the axial direction, L is the total length, and c_0 is the first layer thickness, which is set to 0.1 m in this paper.

The radial discrete expression of the soil temperature field is as follows[12]:

$$r_{\mathrm{s}(j+1)} = r_{\mathrm{s}(j)} \cdot e^{\left(\frac{1\mathrm{n}(r_{\mathrm{s}}/r_{\mathrm{b}})}{n_{\mathrm{s}}}\right)} \tag{7}$$

where n_{s} is the number of radially discrete layers of soil, r_{s} is the radius of the soil far field, and r_{b} is the radius of the borehole.

The implicit difference scheme is used to discretize the fluid, pipeline, backfill material, borehole wall, and soil on the axis to divide them into 10 layers, and the soil is divided into 8 layers by radial discretization. Taking the fluid-side as an example, the fluid-side node network model is established:

For $i = 1$:
$$\frac{C_{\mathrm{f}(i)}}{d\tau} \cdot T^1_{\mathrm{f}(i)} = \frac{1}{R_{\mathrm{fl}(i)}} \cdot T^1_{\mathrm{pi}(i)} + \frac{1}{R_{\mathrm{fh}(i)}} \cdot T^1_{\mathrm{f}(i+1)} - \left(\frac{1}{R_{\mathrm{fl}(i)}} + \frac{1}{R_{\mathrm{fh}(i)}} - \frac{C_{\mathrm{f}(i)}}{d\tau}\right) \cdot T^0_{\mathrm{f}(i)} \tag{8}$$

For $1 < i < n_z$:
$$\frac{C_{\mathrm{f}(i)}}{d\tau} \cdot T^1_{\mathrm{f}(i)} = \frac{1}{R_{\mathrm{fl}(i)}} \cdot T^1_{\mathrm{pi}(i)} + \frac{1}{R_{\mathrm{fh}(i)}} \cdot T^1_{\mathrm{f}(i+1)} + \frac{1}{R_{\mathrm{fh}(i-1)}} \cdot T^1_{\mathrm{f}(i-1)} - \left(\frac{1}{R_{\mathrm{fl}(i)}} + \frac{1}{R_{\mathrm{fh}(i)}} + \frac{1}{R_{\mathrm{fh}(i-1)}} - \frac{C_{\mathrm{f}(i)}}{d\tau}\right) \cdot T^0_{\mathrm{f}(i)} \tag{9}$$

For $i = n_z$:
$$\frac{C_{\mathrm{f}(i)}}{d\tau} \cdot T^1_{\mathrm{f}(i)} = \frac{1}{R_{\mathrm{fl}(i)}} \cdot T^1_{\mathrm{pi}(i)} + \frac{1}{R_{\mathrm{fh}(i-1)}} \cdot T^1_{\mathrm{f}(i-1)} - \left(\frac{1}{R_{\mathrm{fl}(i)}} + \frac{1}{R_{\mathrm{fh}(i-1)}} - \frac{C_{\mathrm{f}(i)}}{d\tau}\right) \cdot T^0_{\mathrm{f}(i)} \tag{10}$$

3. RESULTS AND DISCUSSION

3.1 Basic data

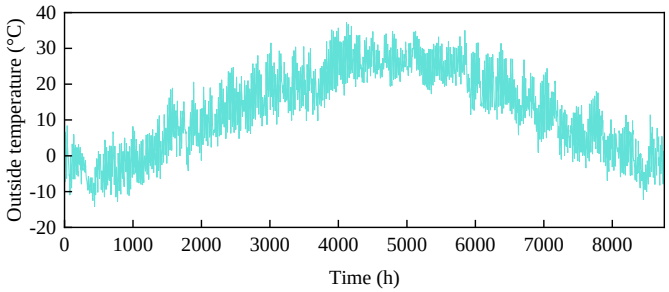

Figure 3: Hourly ambient temperature profiles.

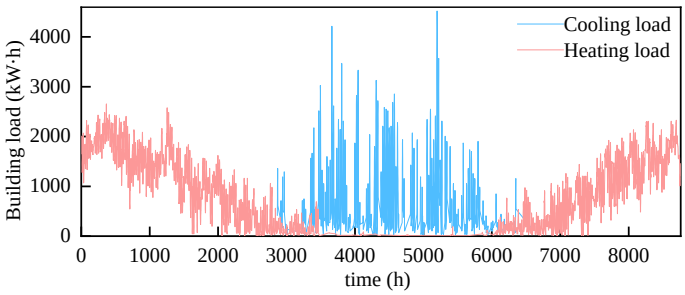

Figure 4: Hourly heating and cooling load distribution of residential buildings.

Figure 3 shows hourly changes in ambient temperature throughout the year. It can be seen that the ambient temperature varies significantly with the seasons. The annual ambient temperature ranges from -14.2 ℃ to 37.2 ℃. The lowest temperature is on January 19, and the highest temperature is on June 21. Figure 4 shows the annual load distribution of the residential community. The heat load demand is mainly in winter, followed by the transitional season of spring and autumn, and the heating load day on January 15 is the highest, reaching 2654.4 kW.

3.2 Dynamic simulation analysis of the system in the heating season

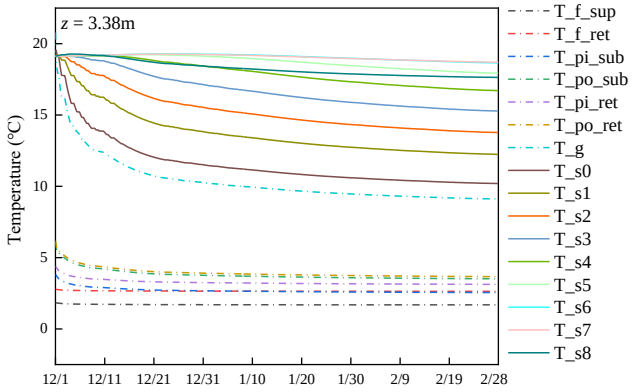

Figure 5: Temperature distribution of each node at *z* = 3.38 m.

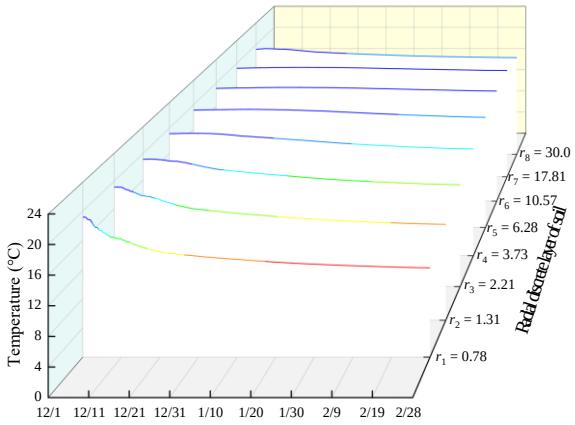

Figure 6: Radial variation of soil temperature field at *z* = 3.38 m.

Figure 5 and Figure 6 show the dynamic changes of the temperature field of soil and other nodes at z = 3.38 m. As can be seen from Figure 5, the temperature of fluid and inner and outer pipe sides change moderately, while the temperature of backfill material is reduced by 11.68 ℃ and radial shallow soil is reduced by 0.56 ℃-9.34 ℃. It is worth noting that the temperature difference not only between the fluid side and the shallow soil is formed, but also between the deep soil and the shallow soil, which results in bidirectional heat transfer in the soil.

The heat transfer fluid does not form a thermal disturbance to the deep soil because of the limited running time, so the soil temperature remained constant from the 6th layer. As can be seen from Figure 6, the soil temperature responds at 2.21 m in the radial direction after the first month, and the temperature decreased by 2.03~5.35 °C. Furthermore, the soil temperature response reaches 3.73 m at the end of the second month, which was 1.07~1.23 °C lower than that of the first month. The soil with a thickness of 6.28 m was affected at the end of the third month, and the temperature decreased by 0.46~1.23 °C compared with the second month. It can be seen that the rate of heat release gradually slows down with time.

3.3 COP

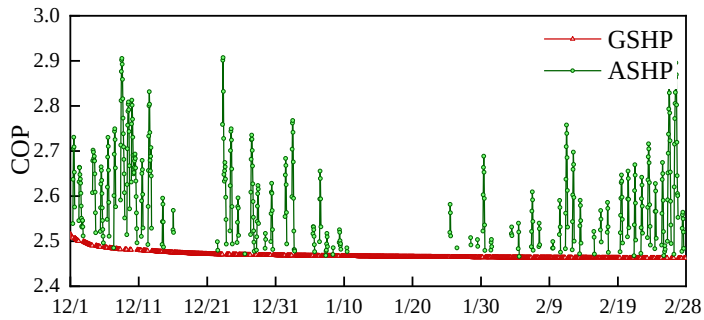

Figure 7: Variation of COP with time for a heating system.

Figure 7 shows the variation of COP for a multi-source integrated district heating system with ambient temperature. It can be seen that the start and stop of the two subsystems (ground source heat pump and air source heat pump) are related to energy efficiency. When the COP of the ground source heat pump is higher than the air source heat pump, the ground source heat pump is started. It is worth mentioning that the COP of the ground source heat pump system decreases slowly as the inlet fluid as the temperature field of the geothermal source side changes. The COP decreases rapidly at the beginning of the heating season, and it is nearly constant during January and February.

3.4 Primary energy consumption

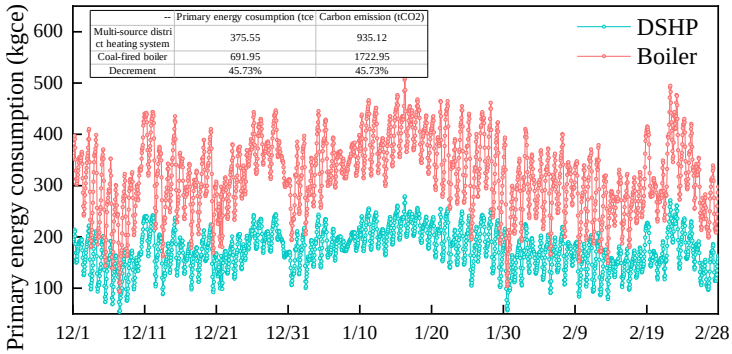

--	Primary energy cosumption (tce	Carbon emission (tCO2)
Multi-source district heating system	375.55	935.12
Coal-fired boiler	691.95	1722.95
Decrement	45.73%	45.73%

Figure 8: Hourly primary energy consumption of the system.

Figure 8 shows the hourly variation of the primary energy consumption for the multi-source district heating system and the traditional boiler system. It can be seen that the primary energy consumption of the integrated energy system is reduced by 316.4 t_{ce} and carbon emissions is reduced by 787.83 t_{CO2} compared with the traditional boiler system. Therefore, the combination of multi-source district heating technology and renewable sourc1e is an efficient technical route to achieve carbon peaking and carbon neutrality.

4. CONCLUSION

A multi-source district heating system integrated with geothermal and air sources is proposed. Then, the simulation model of the single U-tube geothermal exchanger, and the multi-source heat pump system integrated with the ground source air source are developed. The following conclusions can be obtained:

(1) The radial response of the soil temperature field slows down with time, with the temperature decreasing in the latter two months being only 20.05% and 8.59% of the first month.

(2) The operation strategy of the multi-source district heat pump heating system shows the ground source heat pump is on when the ambient temperature is relatively low, while the air source heat pump is on when the ambient temperature is high.

(3) The COP of the ground source heat pump system reduces gradually as the temperature field of the geothermal source side decreases. Additionally, it decreases rapidly at the beginning of the heating season and tends to be constant as time goes on.

(4) The multi-source district heating system reduces primary energy consumption by 316.4 t_{ce} and carbon emissions by 787.83 t_{CO2} compared to coal-fired boilers.

REFERENCES

[1] IEA. 2019 Global Status Report for Buildings and Construction[R]. Global Alliance for Buildings and Construction, 2019.
[2] Xinhua net. More than 170 leaders gather at UN headquarters to sign the Paris Agreement. http://www.xinhuanet.com/world/2016-04/22/c_128922630.htm. 2016-04-22/2022-09-25.
[3] Central People's Government of the People's Republic of China. Opinions of the CPC Central Committee and the State Council on the complete and accurate implementation of the new development concept to do a good job of carbon peaking and carbon neutrality. http://www.gov.cn/xinwen/2021-10/25/content_5644687.htm. 2021-10-25/2022-09-25.
[4] Central People's Government of the People's Republic of China. Plan for Clean Winter Heating in Northern Areas (2017-2021). http://www.gov.cn/xinwen/2017-12/20/content_5248855.htm. 2017-12-20/2022-09-25.
[5] (Central People's Government of the People's Republic of China. The 14th Five-Year Plan for a Modern Energy System. http://www.gov.cn/zhengce/zhengceku/2022-03/23/content_5680759.htm. 2022-1-29/2022-09-25.).
[6] Emmi, G., Zarrella, A. and De Carli, M.: A heat pump coupled with photovoltaic thermal hybrid solar collectors: A case study of a multi-source energy system[J], *Energy Conversion and Management*, (2017), 151: 386-99.
[7] Grossi, I., Dongellini, M., Piazzi, A., et al.: Dynamic modelling and energy performance analysis of an innovative dual-source heat pump system[J], *Applied Thermal Engineering*, (2018), 142: 745-59.
[8] Jia, L., Lu, L., Chen, J., et al.: A novel radiative sky cooling-assisted ground-coupled heat exchanger system to improve thermal and energy efficiency for buildings in hot and humid regions[J], *Applied Energy*, (2022), 322.
[9] Nordgård-Hansen, E., Kishor, N., Midttømme, K., et al.: Case study on optimal design and operation of detached house energy system: Solar, battery, and ground source heat pump[J], *Applied Energy*, (2022), 308.
[10] Zheng, Z., Zhou, J., Xu, F., et al.: Integrated operation of PV assisted ground source heat pump and air source heat pump system: Performance analysis and economic optimization[J], *Energy Conversion and Management*, (2022), 269.
[11] National Standardization Management Committee. GB 21455-2019, Energy efficiency limits and energy efficiency classes for room air conditioners[S]. Beijing：China Standard Publishing House, 2019.
[12] Nguyen, A., Eslami-Nejad, P., Badache, M., et al.: Pressure–enthalpy coupled thermal resistance and capacity model (PH-TRCM) for direct-expansion borehole heat exchangers: Application for supercritical CO_2[J], *Geothermics*, (2018), 76: 50-9.